# Solvent Systems for Industrial-Scale Processing of Spiro-OMeTAD Hole Transport Layer in Perovskite Solar Sells

Isabelli, Fabiano; Di Giacomo, Francesco; Gorter, Harrie; Brunetti, Francesca; Groen, Pim; Andriessen, Ronn; Galagan, Yulia

**DOI**
10.1021/acsaem.8b01122

**Publication date**
2018

**Document Version**
Final published version

**Published in**
ACS Applied Energy Materials

**Citation (APA)**
Isabelli, F., Di Giacomo, F., Gorter, H., Brunetti, F., Groen, P., Andriessen, R., & Galagan, Y. (2018). Solvent Systems for Industrial-Scale Processing of Spiro-OMeTAD Hole Transport Layer in Perovskite Solar Sells. *ACS Applied Energy Materials*, *1*(11), 6056-6063. https://doi.org/10.1021/acsaem.8b01122

ACS APPLIED ENERGY MATERIALS
Cite This: ACS Appl. Energy Mater. 2018, 1, 6056−6063
Article
www.acsaem.org

# Solvent Systems for Industrial-Scale Processing of Spiro-OMeTAD Hole Transport Layer in Perovskite Solar Sells

Fabiano Isabelli,[†,‡] Francesco Di Giacomo,[†] Harrie Gorter,[†] Francesca Brunetti,[‡] Pim Groen,[†,§] Ronn Andriessen,[†] and Yulia Galagan*[,†]

[†]Holst Centre, Solliance, High Tech Campus 21, 5656 AE, Eindhoven, The Netherlands

[‡]CHOSE—Centre for Hybrid and Organic Solar Energy, Department of Electronic Engineering, University of Rome Tor Vergata, via del Politecnico 1, 00133 Rome, Italy

[§]Faculty of Aerospace Engineering, Delft University, Kluyverweg 1, 2629 HS Delft, The Netherlands

Supporting Information



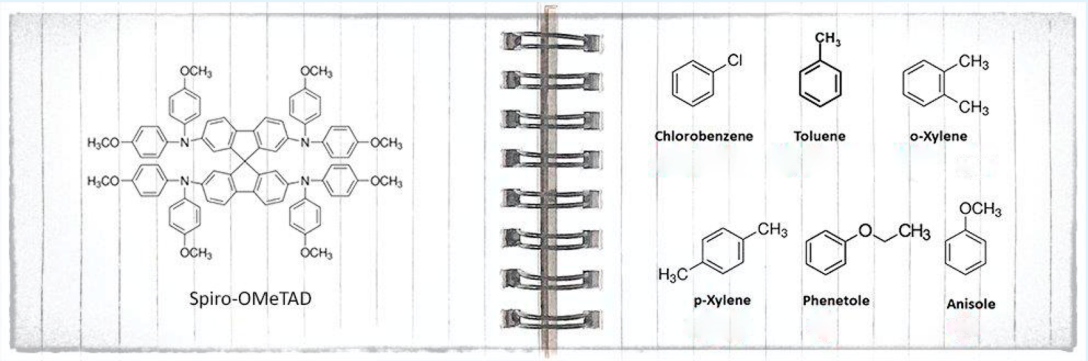


**ABSTRACT:** Current laboratory-scale fabrication of perovskite solar cells involves the use of toxic solvents in the different fabrication steps. The aim of this research is to find a nontoxic alternative to chlorobenzene used for the deposition of hole transport material (HTM) spiro-OMeTAD. The initial selection of the solvents compatible with industrial manufacturing was performed based on the Hansen solubility model and further verified in a series of solubility tests, because the additives used in the HTM ink, such as lithium bis(trifluoromethanesulfonimidate) (Li-TFSI) and *tert*-butylpyridine (4-TBP), also have a significant influence on the properties of the final solution. Furthermore, selected solvents were tested on the compatibility with the underlying perovskite layer, which should remain unaffected after the spiro-OMeTAD deposition. A final selection of solvents was tested by the manufacturing of the complete perovskite solar cells. Power conversion efficiency (PCE) and layer quality, as well as possible health issues and environmental concerns, influenced the final selection for future potential industrial processing. The research demonstrated that replacement of chlorobenzene (CB) by *p*-xylene leads to identical PCEs of the devices, thereby showing that a toxic solvent can be replaced by a nontoxic and industrially compatible one. To prove that the selected solvent is suitable for future large-area coatings, the coatability of the ink was tested in blade-coating deposition. Devices manufactured using blade coating demonstrated identical PCEs to spin-coated devices, which is final proof of the suitability of the selected solvent system.

**KEYWORDS:** *perovskite solar cells, industrial-scale manufacturing, scaling up, nontoxic solvent system, nonhazardous solvents, hole transport material, HTM, spiro-OMeTAD*

## INTRODUCTION

Nowadays, solar cells are becoming one of the most widespread solutions to replace conventional energy sources, such as coal and oil, that will reduce $CO_2$ emission and prevent the risk of global warming. In order to enable green energy sources, such as solar cells, manufacturing technologies should avoid expensive materials and process steps, reduce energy consumption during manufacturing, and eliminate harmful materials, such as toxic solvents. Currently, silicon-based technologies are the most commonly used for photovoltaic application because of high know-how, well established and reliable manufacturing process, high power conversion efficiency (PCE), and a good lifetime of the Si-based PV modules.[1] However, Si-based PV modules, produced using the Czochralski process, are expensive because of the extremely high purity wafers and high temperature furnaces involved (which are high energy consuming).[2] In the past few years, perovskite solar cells (PSCs) made a breakthrough in

Received: July 10, 2018
Accepted: October 1, 2018
Published: October 1, 2018





DOI: 10.1021/acsaem.8b01122
ACS Appl. Energy Mater. 2018, 1, 6056−6063

Table 1. Hansen Parameters and Hansen Distance Relative to Chlorobenzene

| solvent | Hansen solubility parameters | | | | | Hansen distance |
|---|---|---|---|---|---|---|
| | interaction radius | δD | δP | δH | molar vol ($cm^3$/mol) | |
| chlorobenzene | 19.6 | 19 | 4.3 | 2 | 101.7 | 0.0 |
| tetralin | 19.9 | 19.6 | 2 | 2.9 | 136.4 | 2.75 |
| phenetole | 19.4 | 18.4 | 4.5 | 4.0 | 126.5 | 2.34 |
| toluene | 18.2 | 18 | 1.4 | 2 | 106.3 | 3.52 |
| *o*-xylene | 18.1 | 17.8 | 1 | 3.1 | 120.6 | 4.23 |
| *p*-xylene | 18.1 | 16.6 | 7.0 | 2.0 | 123.6 | 5.54 |
| cyclohexanone | 19.6 | 17.8 | 6.3 | 5.1 | 104.1 | 4.43 |
| acetophenone | 21.7 | 19.6 | 8.6 | 3.7 | 117.1 | 4.78 |
| indane | 21.8 | 19.7 | 7.3 | 5.8 | 122.5 | 5.04 |
| anisole (methoxybenzene) | 19.5 | 17.8 | 4.1 | 6.7 | 108.7 | 5.28 |
| limonene (info Dow Chemicals) | 16.5 | 16.5 | 0.6 | 0 | 162.1 | 6.53 |
| 1,2-dimethoxybenzene (Veratrole) | 21.8 | 19.2 | 4.4 | 9.4 | 127.5 | 7.41 |
| oleic acid | 17.4 | 16.0 | 2.8 | 6.2 | 318.4 | 7.48 |
| THF | 19.5 | 16.8 | 5.7 | 8 | 81.1 | 7.57 |
| PGMEA | 18.4 | 16.1 | 6.1 | 6.6 | 136.7 | 7.62 |
| cyclopentanone | 22.1 | 17.9 | 11.9 | 5.2 | 88.5 | 8.53 |
| isobutyl acetate | 16.8 | 15.1 | 3.7 | 6.3 | 134.4 | 8.88 |

photovoltaic technologies. Unique properties of perovskite semiconductors, such as high absorption coefficient, long charge diffusion length, tunable band gap, and very low nonradiative recombination made these materials very attractive for PV applications.[3,4] Moreover, fast progress in the record PCE, from 6.5% in 2011[5] up to 22.7% in 2018,[6] made perovskites competitive with conventional PV technologies. In addition to high PCE and attractive physical properties, perovskite solar cells can be produced from solution at relatively low temperatures (typically <150 °C) using a variety of deposition methods and made from abundantly available cheap materials,[7] providing a short energy payback time for perovskite PV manufacturing[8] and supporting R2R processing on flexile substrates. Therefore, a lot of studies now are focused on the upscaling of PSCs[9−11] in order to obtain large-area devices and thereby to start mass production of perovskite photovoltaics. Despite significant progress in this field, the fabrication processes still often involve toxic halogenated solvents classified as carcinogenic−mutagenic−reprotoxic (CMR), which are harmful to both health and the environment. The usage of hazardous solvents in industrial R2R manufacturing is under regulatory consideration and requires that additional steps are taken for the storage, deposition, solvent removal, and drying, to keep the mission level within the mandated limit. Manufacturing from non-hazardous solvents will allow a safe and environmentally friendly process.

A typical device stack of PSCs consists of at least three layers produced from solutions. Therefore, solvents selection for deposition of each functional layer is an important step. A selected solvent system for each functional layer, which should be not hazardous to meet the requirement of industrial manufacturing, also should not damage the layers underneath and should provide a high PCE of the devices. For example, fabrication of perovskite layers typically involves utilization of a hazardous solvent such as dimethylformamide (DMF). Several alternatives to DMF have been reported, such as acetonitrile/methylamine mixture,[12] or blends of γ-butyrolactone (GBL) with cyclic carbonates, alcohols, or acids.[13] However, due to the very low boiling point of methylamine and high flammability of acetonitrile, or the legislative status of GBL, these solvents are not favorable for industrial mass manufacturing. Wang et al.[14] have demonstrated a nontoxic and industry-compatible solvent system for perovskite precursors. Furthermore, an electron transport layer (ETL), e.g., $SnO_2$, can be deposited from a water dispersion which is fully compatible with an industrial-scale production.[15] By contrast, the deposition process of the spiro-OMeTAD hole transport layer (HTL) involves chlorobenzene (CB) as a solvent. Replacement of CB in the HTL solution is required for industrial manufacturing to reduce the environmental impact and personal health issues. In literature, some alternative solvents have been investigated showing promising results. As an example, Bu et al.[16] obtained 19.43% PCE on small-area devices (0.16 $cm^2$) by replacing CB with ethyl acetate (EA). However, EA shows some limits for large-area industrial device fabrication because of the low boiling point (77.1 °C), and high volatility. Manufacturing technologies using low boiling point solvents involve control measures in order to avoid occurrence of explosive vapor mixtures, and therefore very volatile solvents are not preferred in the manufacturing process. Recently, anisole was used as an antisolvent in perovskite deposition and as a solvent for the hole transporter material (HTM).[17] However, we believe that the use of a solvent with lower surface energy should be favored for the sake of large-area coating uniformity. Still, the search for a good alternative, to replace CB in spiro-OMeTAD solution, maintaining, high PCE and a good coatability over the large areas, is needed for future industrial manufacturing. This solvent could also be used to replace CB in other perovskite structure (i.e., PCBM or PTAA), widening the scope of this research. To meet the requirements of industrial manufacturing, an alternative solvent system should fulfill the following criteria: (I) Spiro-OMeTAD has to be soluble in the solvent, (II) the solvent should not be in the CMR list, (III) the solvent does not disrupt the other layers which are underneath, (IV) there is a reduced explosion risk of the solvent, (V) a low surface energy of the solvent is needed to provide good uniformity using industrially compatible coating methods, and, obviously, (VI) solar cell devices have to yield good PCE. In this work, we will demonstrate the use of



DOI: 10.1021/acsaem.8b01122
ACS Appl. Energy Mater. 2018, 1, 6056−6063

industrially compatible solvents for HTM ink that satisfy the above conditions.

## RESULTS AND DISCUSSION

The initial alternative solvent selection for the spiro-OMeTAD was done using the so-called Hansen solubility model.[18] Within the Hansen model, each chemical compound has a unique set of Hansen parameters that represent different intramolecular interactions and give a 3D coordinate which comprises polar, disperse, and hydrogen bonding values. To make a theoretical estimation of which solvent can potentially dissolve a certain molecule, the solvent with 3D coordinates should be close to the molecule in the three-dimensional Hansen space. One of the problems for spiro-OMeTAD is that its Hansen parameters are unknown. From the knowledge that spiro-OMeTAD is well dissolved in CB, it is assumed the Hansen parameters of spiro-OMeTAD are close to that of CB. Using CB as a reference, one can calculate which solvents are close to chlorobenzene, as shown in Table 1. The Hansen distance presented in Table 1 is the distance between the sphere of the selected solvent on a three-dimensional Hansen graph and the center of the sphere of CB (with the assumption that it is also the center of the sphere for spiro-OMeTAD). This is however only a rough guideline. The Hansen model is rather accurate for aliphatic compounds, but for aromatic and ionizing compounds it is much less accurate. Looking at the structure of the spiro-OMeTAD (Figure 1), one can see it comprises 12 aromatic rings, with eight methoxy groups and four amine groups. Based on this, it is expected that aromatic solvents in Table 1 with a small polarity might do well as a solvent. Selected aromatic solvents were supplemented by few solvents which do not contain a ring structure, e.g., isobutyl acetate and propylene glycol methyl ether acetate (PGMEA).

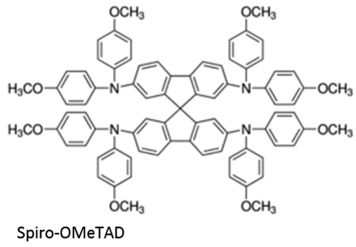


**Figure 1.** Molecular structure of spiro-OMeTAD.

To start an investigation of the alternative solvent systems for industrial use, it is necessary to study the solubility of spiro-OMeTAD in various solvents preselected using the Hansen solubility model. The concentration of spiro-OMeTAD was considered at 30 mg·mL$^{-1}$. Although spin coating involves a highly concentrated solution (80 mg·mL$^{-1}$ or higher), this deposition method is not suitable for industrial manufacturing. Focusing on slot die coating as a future deposition technique, or doctor blading as an intermediate alternative, the concentration of the solution should not exceed 30 mg·mL$^{-1}$ (it is typically 20 mg·mL$^{-1}$ or lower) for the final dry layer thickness of about 200 nm. This low concentration range allows wider varieties of the possible solvents to be used for the spiro-OMeTAD deposition.

Testing the solubility of spiro-OMeTAD in preselected solvents revealed that the nonaromatic solvents isobutyl acetate and PGMEA do not dissolve the spiro-OMeTAD (see Table 2). Moreover, limonene and oleic acid also do not dissolve the spiro-OMeTAD. Unexpectedly the acetophenone gives a yellow transparent solution but with clearly visible black precipitates, possibly the result of an interaction with an impurity in the acetophenone. Although a number of solvents suitable for dissolving spiro-OMeTAD were identified, the final solution of the manufacturing spiro- OMeTAD hole-transporting layer typically contains bis(trifluoromethylsulfonyl)-imide (Li-TFSI) salt and 4-*tert*-butylpyridine (4-TBP) in order to oxidize spiro-OMeTAD and improve hole mobility, and thereby improve performance of the devices. The presence of these additives in the solutions made with alternative solvents also should be evaluated. The Li-TFSI has a clear impact on the stability of the solutions. Some solutions turn from bright yellow to an orange/brown color; some solutions turn hazy, indicating a presence of the precipitates in the solution. Upon

**Table 2. Effect of Dissolution Experiment of Spiro-OMeTAD at 30 mg/mL with Additives**

| | | step 1 | step 2 | step 3 | step 4 |
|---|---|---|---|---|---|
| solvent | Hansen radius to CB ($\sqrt{MPa}$) | spiro-OMeTAD at 30mg/mL | add Li-TFSI (in acetonitrile) | add 4-TBP | compatibility perovskite |
| chlorobenzene | 0.00 | yellow, clear | yellow, clear | yellow, clear | good |
| tetralin | 2.75 | yellow, clear | orange, clear | yellow, clear | |
| phenetole | 2.34 | yellow, clear | brown, clear | orange, clear | small interaction |
| toluene | 3.52 | yellow, clear | orange, hazy | yellow, clear | good |
| *o*-xylene | 4.23 | yellow, clear | orange, hazy | yellow, clear | good |
| *p*-xylene | 5.54 | yellow, clear | orange, hazy | yellow, clear | good |
| cyclohexanone | 4.43 | yellow, clear | yellow, clear | yellow, clear | dissolve |
| acetophenone | 4.78 | yellow + black precip. | yellow + black precip. | yellow + black precip. | |
| indane | 5.04 | yellow, clear | yellow, hazy | yellow, clear | dissolve |
| anisole | 5.28 | yellow, clear | orange, hazy | yellow, clear | good |
| limonene | 6.53 | not dissolved | | | |
| veratrole | 7.41 | yellow, clear | yellow, clear | yellow, clear | |
| oleic acid | 7.48 | not dissolved | | | |
| THF | 7.57 | yellow, clear | yellow, clear | yellow, clear | |
| PGMEA | 7.62 | not dissolved | | | |
| cyclopentanone | 8.53 | yellow, clear | orange, clear | yellow, clear | dissolve |
| isobutyl acetate | 8.88 | not dissolved | | | |



DOI: 10.1021/acsaem.8b01122
ACS Appl. Energy Mater. 2018, 1, 6056−6063

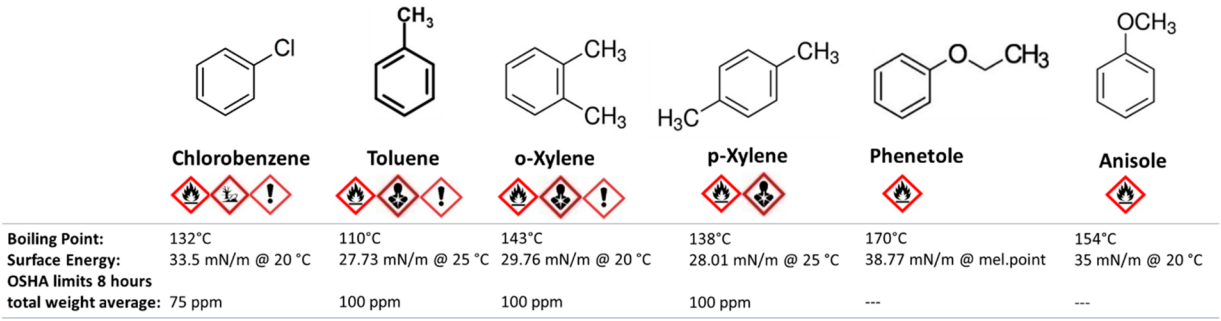


**Figure 2.** Solvents selected for the devices manufacturing and the properties of the solvents.

adding the 4-TBP, orange solutions become bright yellow again and a haziness disappears, except the phenetole-based solution, which turns to clear orange, and acetophenone-based solution, where black precipitates remain in the solution. This effect is explained by the ability of 4-TBP to improve the solubility of Li-TFSI in the aromatic solvent, preventing its precipitation.[19]

A next criterion in the solvent system selection is a compatibility of the solvents with perovskite layer which should remain unaffected after deposition of spiro-OMeTAD on top of it. To check the interaction between the perovskite and selected solvents, a few drops of the solvents were deposited on the coated perovskite layers (step 4). For this experiment, only the solvents which passed the previous stages were evaluated. Therefore, acetophenone, which forms black precipitates in the presence of Li-TFSI and 4-TBP, was not further evaluated. Also, despite quite a broad list of solvents that passed the selection criteria, some of them were discarded because their boiling points are not compatible with R2R either with deposition or in drying. Thus, THF owning the boiling point of 66 °C is not suitable for slot die coating, because the solvent will start evaporating before the wet layer reaches the dryer in an R2R line. This will significantly influence a perovskite crystallization process and the layer uniformity. Opposite, solvents with very high boiling points, such as veratrole and tetralin (boiling points are 206 and 208 °C, respectively), also will have problems with crystallization and drying; these solvents might not completely evaporate during the deposition because of (i) the temperature limits of 140 °C determined by PET substrate, (ii) a limited length of the drier, and (iii) high speed at R2R deposition. Therefore, THF, veratrole, and tetralin were discarded from further evaluation. The experiment reveals that several solvents, cyclohexanone, anisole, and indane, destroy the perovskite layer. Phenetole has small (insignificant) interaction with the perovskite layer, while other solvents do not interact with the perovskite layer. Thus, solvents which pass all preliminary evaluation steps (see Figure 2) are toluene, *o*-xylene, *p*-xylene, phenetol, anisole, and reference chlorobenzene.

The safety level of the remaining solvent has furthermore been evaluated in order to find less hazardous alternatives for chlorobenzene. In Figure 2 the alternative solvents are listed with their chemical structures, CLP hazard pictograms, boiling points, surface tensions, and the exposure limit for 8 h (according to the U.S. Occupational Safety and Health Administration[20]). All of the selected solvents have an aromatic ring with one, or more side groups and have boiling points in the range from 110 °C (toluene) to 170 °C (phenetole). Regarding the toxicity issue, *p*-xylene, phenetole, and anisole are not included in the CMR list, displaying a lower health risk compared with other ones (CB, *o*-xylene, and toluene). Still, safety precautions should be still implemented for the manufacturing environment to avoid given the similar exposure limit reported.

The next step in the evaluation of alternative solvents is a manufacturing of the devices, where spiro-OMeTAD is deposited from the selected solvents. As has been discussed earlier, to be aimed in a future slot die coating, the concentration of spiro-OMeTAD in the investigated solvents was 30 mg·mL$^{-1}$. However, a slot die coating (or doctor blading) of spiro-OMeTAD using investigating solutions may lead to misleading results, because the reference devices are produced by spin coating. On the other hand, comparison of the investigated solutions by spin-coated deposition cannot provide a reliable comparison with the reference because the reference devices manufactured using CB have a much higher concentration of spiro-OMeTAD (80 mg·ml$^{-1}$). Increasing the concentration of spiro-OMeTAD in alternative solvents might discard many of them due to limited solubility of the spiro-OMeTAD, which will lead us out of the main purpose of this study: to find a solvent system for slot die or blade coating of spiro-OMeTAD. Therefore, to have a credible comparison with the reference, the concentration of reference CB solution was also reduced to 30 mg·mL$^{-1}$. Reduction of the concentration of spiro-OMeTAD in the reference solution required reoptimization of deposition parameters (spin speed and time) in order to obtain the thickness of HTL of at least 150 nm to guarantee good PCE. Therefore, spiro-OMeTAD deposited from 30 mg·mL$^{-1}$ solutions of CB in the reference stack of glass/ITO/$SnO_2$/$Cs_{0.05}(MA_{0.17}FA_{0.83})_{0.95}Pb(I_{0.27}Br_{0.73})_3$/spiro-OMeTAD/Au was deposited using different spin speeds, as shown in Figure 1S. It is observed that for a spinning time of 60 s, devices with 2000, 1500, and 1000 rpm show approximately the same PCEs, but a significantly lower layer thickness. Keeping a layer thickness in the range of 200 nm is essential for future doctor blading and slot die coating. Therefore, in order to increase the thickness of the layer, spiro-OMeTAD was deposited with a lower spin speed: 500 rpm. The devices with 500 rpm deposition speed exhibit drying problems for 60 s spinning, resulting in a non-uniform layer. For this reason, spinning time was increased to 120 s, allowing spiro-OMeTAD solution to dry uniformly. Although devices with spiro-OMeTAD layer produced from 30 mg·mL$^{-1}$ solution at 500 rpm have higher hysteresis compared with other devices, these devices have the highest stabilized efficiency and demonstrate a designed layer thickness of 200 nm. Therefore, a deposition speed of 500 rpm and a deposition time of 120 s were used for the further investigation of the


DOI: 10.1021/acsaem.8b01122
ACS Appl. Energy Mater. 2018, 1, 6056−6063

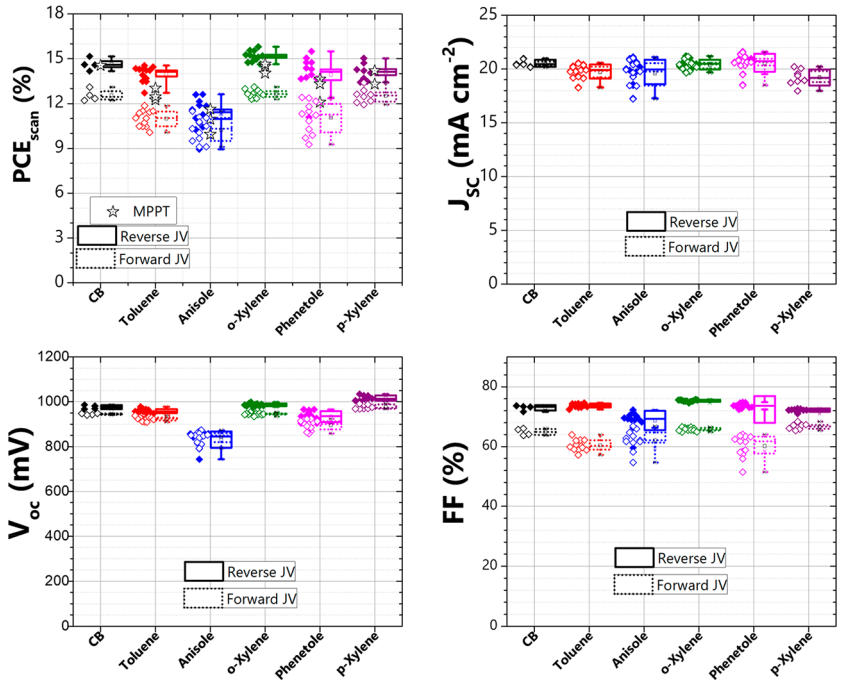


**Figure 3.** PV characteristics of the devices (glass/ITO/$SnO_2$/$Cs_{0.05}(MA_{0.17}FA_{0.83})_{0.95}Pb(I_{0.27}Br_{0.73})_3$/spiro-OMeTAD/Au) manufactured using different solvents for deposition of spiro-OMeTAD.

alternative solvents. The performance of the devices manufactured using alternative solvents will be compared to the performance of the devices with the spiro-OMeTAD layer produced from 30 mg·mL$^{-1}$ CB solution at 500 rpm.

The PV characteristics of the devices fabricated with alternative solvents are depicted in Figure 3. It is evident that *o*-xylene, phenetole, and *p*-xylene demonstrate PCEs as good as CB. Devices made from anisole show the poorest PCE among the tested solvents, and in addition, it displays a notable poor layer uniformity (see Figure 4). Toluene shows better

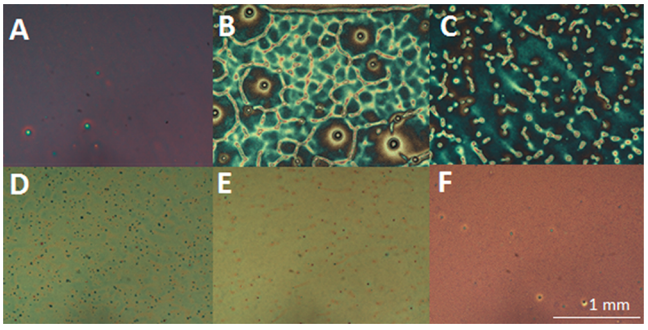


**Figure 4.** Optical microscope images of spiro-OMeTAD layer deposited from different solvents: (A) chlorobenzene, (B) anisole, (C) phenetole, (D) *o*-xylene, (E) *p*-xylene, and (F) toluene.

PCE than anisole but still is not as good as chlorobenzene and other solvents. A hysteresis observed in the devices, even using standard solvent CB, is also widely described in literature when devices with an identical n−i−p configuration are used.[21,22] It is well accepted that one of the causes of hysteresis is the issue of interfaces. In order to have high PCE and low hysteresis, it is essential to provide unobstructed pathways for carriers from absorber to both electrodes. The hysteresis due to the ITO−$SnO_2$ interface is intensively discussed in literature,[23] and some solutions to reduce the hysteresis were proposed via surface modification.[24] Furthermore, a lot of optimizations of perovskite layer were done in order to reduce hysteresis.[25] However, from Figure 3 it is obvious, that changing a solvent for spiro-OMeTAD results in the increased hysteresis in some cases, e.g., when toluene, *o*-xylene, or phenetole is used. Most likely, change of a solvent composition leads to the modification of the perovskite/spiro-OMeTAD interface and it leads to increased hysteresis. Here at least two parameters can be responsible for this behavior: layer quality and slight energy level modification of spiro-OMeTAD when deposited from another solvent. The defects at the interfaces act as effective recombination centers leading to dropping in efficiency and increasing the hysteresis. Thus, spiro-OMeTAD layer quality seems to be the most important parameter and required additional investigation. To further evaluate a suitability of the alternative solvents, the thicknesses and layer uniformity of the spiro-OMeTAD layers deposited from different solvents were investigated.

In Figure 4 the microscope images of spiro-OMeTAD layers deposited from different solvents are presented. Anisole- and phenetole-based layers exhibit many defects compared to the layers produced from CB. The defects in these layers are caused by two reasons. First of all is due to the relatively high surface tensions of these two solvents, which are higher than that of CB (see Figure 2). Second, SEM EDX analysis (see Figure S2) reveals that inhomogeneities in HTL layers produced from anisole and phenetole are mainly composed of carbon. This can be attributed to the nondissolved cluster of spiro-OMeTAD particles into the solvents. Furthermore, an investigation of the layer thicknesses reveals that in addition to the defects in the anisole- and phenetole-based layers, the HTL layers produced from these solvents have a lower layer thickness. This is in line with our findings, that the defects in the layers are nondissolved particles of spiro-OMeTAD. As a result, the concentration of spiro-OMeTAD in the solution is lower, resulting in lower layer thickness. On the other hand,


DOI: 10.1021/acsaem.8b01122
ACS Appl. Energy Mater. 2018, 1, 6056−6063

the thickness of the layer deposited by spin coating also depends on the surface tension of the ink, which also can be an explanation of the insufficient layer thicknesses. These observations make anisole and phenetole less preferred solvents for spiro-OMeTAD. Other solvents, *o*-xylene, *p*-xylene, and toluene, do not show a significant difference in layer uniformity compare to the CB-produced layer. Furthermore, with a good PCE, *o*-xylene demonstrates a layer thickness of 145 nm, which is slightly below the set threshold. At the opposite end, a toluene-based layer results in a 215 nm thickness, while devices have slightly lower PCEs. Finally, the *p*-xylene-based layer, with the layer thickness of 200 nm, is the closest to the reference in terms of layer thickness and the PCE of the devices. The final point in the selection of the best alternative solvent for spiro-OMeTAD is toxicity. Both *o*-xylene and toluene are in the CMR list, making *p*-xylene the best choice for the industrial deposition of spiro-OMeTAD and replacement of CB.

After selection of *p*-xylene as an alternative solvent, one more issue of industrial compatibility needs to be solved. The spiro-OMeTAD layer deposited by spin coating does not require any thermal annealing after the deposition, because the solvent evaporates during spin coating. However, in an industrial R2R coating system, the wet layer is usually dried in a furnace to evaporate solvents because R2R deposition occurs at a high speed, requiring complete removal of the solvent before the coiling. Therefore, further investigations have been conducted to study the effect of thermal annealing after deposition of spiro-OMeTAD in order to determine the process window for future R2R or S2S depositions. A temperature range from room temperature (RT) to 120 °C with the step of 20 °C is selected to investigate the drying effect for spiro-OMeTAD. The following temperatures were applied for 5 min: RT, 40 °C, 60 °C, 80 °C, 100 °C, and 120 °C. The PCEs of the devices are shown in Figure 5a, and the

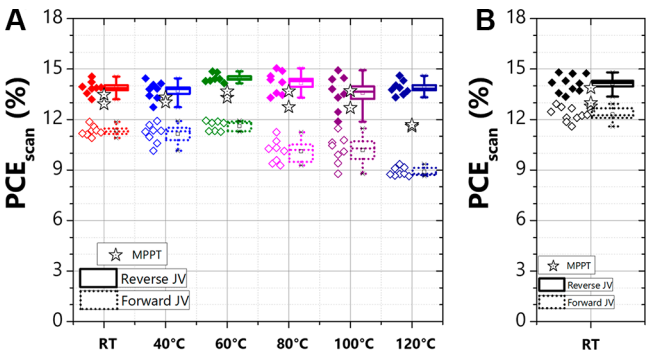


**Figure 5.** PCE of the perovskite solar cells manufactured using *p*-xylene for the deposition of spiro-oMeTAD (A) using spin coating with different postannealing temperatures after the deposition of spiro-OMeTAD and (B) using doctor blading for spiro-OMeTAD deposition.

other IV paraments are presented in Figure S3. It is evident that the thermal step does not degrade a solar cell's performance until 60 °C. Performance of the devices dried at 80−100 °C could be still acceptable, but a remarkable hysteresis is present in IV parameters when devices are measured at reverse and forward scans, even if PCE degradation is not evident. Above 100 °C, the drying process affects performance and significantly decreases the PCE and introduces bigger hysteresis than those observed below 100 °C. Obtained results are in line with the literature, where severe morphological deformations (i.e., crystallization) in the spiro-OMeTAD layer are observed when devices are heated above 80 °C.[26,27] Degradation in the devices with spiro-OMeTAD as the HTM is mainly due to the modification of the interface between the perovskite and spiro-OMeTAD at high temperature. The presence of MA in the perovskite structure speeds up the degradation of the devices compared to the cells not containing MA (e.g., $FA_{0.85}Cs_{0.15}PbI_3$).[26] Thus, our results reveal that the preferable process window for drying of spiro-OMeTAD is from RT up to 60 °C to ensure good PCE and limited hysteresis. Drying at the temperature of 80 °C and higher leads to the degradation of the devices, while heating at the temperature above 100 °C should be completely avoided to guarantee a long lifetime to the devices.

Performed study advises an alternative nonhazardous solvent for deposition of hole-transporting material spiro-OMeTAD, which can be very important for future industrial manufacturing of perovskite solar cells. Although the solvent system for the HTM solution was proposed and the compatibility of the solution with device stacking was proven by device manufacturing, spin-coating technique was used in the study. In most of the cases coating inks used in spin coating are compatible with other deposition methods;[10] postprocessing and drying methods are usually different in alternative coating methods such us blade coating or slot die coating. Thus, in order to prove that *p*-xylene is a suitable solvent for spiro-OMeTAD to be used in a large-area coating process, a test with the blade-coating technique has been realized. However, large-area coating might create difficulties in comparing the results, because more than one parameter will be changed, including the device dimension. Therefore, blade coating was realized on the identical substrates with the same device design and the same device architecture. To have a clear comparison, only two connected parameters were changed: deposition and drying of spiro-OMeTAD. All other parameters including technologies for deposition of all other layers remain the same. To obtain uniform coverage, spiro-OMeTAD concentration in *p*-xylene has been furtherly decreased up to 20 mg·mL$^{-1}$. As shown in Figure 5b, blade-coated devices perform as good as spin-coated ones (see Figure S4 for all IV parameters). The performed experiment confirms suitability of the developed nonhazardous solvent system for the deposition of spiro-OMeTAD by both spin-coating and blade-coating processes. It confirms that the developed solvent system for spiro-OMeTAD can be further transferred to industrial processes such as blade coating or slot die coating.

The work contributes for enabling future technologies with a safe and environmentally friendly deposition of the functional layers. Combination of the developed technology with nonhazardous deposition of other functional layers will speed up commercialization of perovskite solar cells. Although there are some debates regarding the economic aspects of usage of spiro-OMeTAD, the price on this material will go down together with the development of reliable industrial manufacturing, and therefore the current study made a significant contribution for it. Moreover, alternative HTM materials which are currently under development have the same issues, because some of those materials are also expensive (P3HT, PTAA, and so on), and most of them are also deposited from toxic solvent. Therefore, the approach for selection of the alternative solvent presented in the current study is kind of a


DOI: 10.1021/acsaem.8b01122
ACS Appl. Energy Mater. 2018, 1, 6056−6063

generic approach and can be adapted for other hole-transporting materials in the future.

## CONCLUSIONS

There is a need to replace hazardous solvents involved in PSCs fabrication when moving from small devices to large-area fabrication. This study identified the nonhazardous alternatives to CB that could be used for the deposition of spiro-OMeTAD (and potentially also for other ink based on CB such as PCBM). A selection of the alternative solvents was realized using the Hansen solubility method to define a first set of candidates. Successively, spiro-OMeTAD underwent the series of solubility tests, and then the solvents were tested in terms of compatibility with the perovskite layer. And, finally, the solvents that were able to pass the preselection stage were tested in PSCs manufacturing. Among all alternative solvents, *p*-xylene was identified as one of the best candidates to replace CB: it demonstrates good PCE, good layer uniformity, low toxicity, and the possibility to provide the required layer thickness. PCEs of the devices achieved with *p*-xylene are comparable with PCEs of the devices made from CB. Thanks to the favorable low surface energy of the *p*-xylene, it allowed the use of blade coating without further PCE losses. In addition, the thermal annealing has been investigated in order to apply this step to large-area fabrication. The drying temperature of 60 °C was the most favorable for spiro-OMeTAD allowing solvents evaporation and not affecting the devices' performance. The temperatures in the range from 60 to 100 °C can be accepted, although significant IV hysteresis was introduced. Higher temperatures (above 100 °C) lead to the significant drop in PCE and big hysteresis in IV parameters. Testing with blade coating confirms that PCE compared to spin coating from CB can be obtained with spiro-OMeTAD in *p*-xylene. This study provides a comprehensive investigation of alternative solvents and developed a technology for the deposition of spiro-OMeTAD, where both nonhazardous solvent and drying regime are compatible with future industrial manufacturing. The outcome of this study will help to make progress in the field of upscaling and industrialization of perovskite solar cells by S2S and R2R manufacturing.

## EXPERIMENTAL SECTION

**Device Fabrication.** For manufacturing of the devices glass substrates of 3 cm × 3 cm with patterned ITO electrodes were purchased from Naranjo. ITO-coated glass substrates were cleaned, followed by 5 min rinsing with Extran solution, deionized water, and isopropanol (IPA), respectively. Then, substrates were dried using a dry-air gas flow. After cleaning, UV/Ozone treatment took place for 30 min. A tin oxide ($SnO_2$) nanoparticle solution (15 wt %), purchased from Alfa Aesar, was diluted in 1:5 ratio with deionized water and left stirring for 10 min at RT. A tin oxide coating was made using 60 μL of the dispersion per substrate and spin coating at 2500 rpm. After deposition, thermal annealing was executed at 150 °C for 10 min. The $SnO_2$ layer's thickness was 30−40 nm. Perovskite precursor solution was prepared by first making two solutions and dissolving these separately for 1 h and after mixing them together. The first solution consists of 2.88 g of lead iodide ($PbI_2$, from TCI), 0.86 g of formamidinium iodide ((FA)I, where FA = $CH(NH_2)_2$; from Sigma-Aldrich), 0.184 g of lead bromide ($PbBr_2$, from TCI), and 0.112 g of methylammonium bromide ((MA)Br, where MA = $CH_3NH_3$; from Greatcell Solar) dissolved in 4.5 mL of DMF and 0.5 mL of DMSO at RT. The second solution consists of 0.195 g of cesium iodide (CsI, from Sigma-Aldrich) dissolved in 0.5 mL of DMSO. After 1 h, 0.2 mL of CsI solution was added into the first solution.[28] Solutions were mixed together, in order to fabricate the mixed-cation, mixed-halide perovskite phase $Cs_{0.05}(MA_{0.15}FA_{0.85})_{0.95}PbI_{2.55}Br_{0.45}$. A 100 μL aliquot of perovskite solution was spin-coated first at 1000 rpm for 10 s with an acceleration of 500 rpm $s^{-1}$ and then continued spinning at 5000 rpm for 30 s with an acceleration of 2000 rpm $s^{-1}$. After 25 s of spinning, 170 μL of CB was dropped onto the substrates. The spiro-OMeTAD solution (80 mg of spiro-OMeTAD (Lumtec), 28 μL of 4-*tert*-butylpyridine (TBP), and 17.5 μL of a 520 mg·$mL^{-1}$ Li-TFSI solution in acetonitrile were added to 1 mL of chlorobenzene. The concentration of the components for 30 mg·$mL^{-1}$ solutions was reduced accordingly. Dissolution of TBP and Li-TFSI occurred at 60 °C. HTL deposition involved dispensing 60 μL of spiro-OMeTAD solution at different spinning speeds and times depending on the solution used. For 80 mg·$mL^{-1}$ solution, it was 2000 rpm for 60 s, while for 30 mg·$mL^{-1}$ it was 500 rpm for 120 s. Finally, 100 nm gold top contacts were evaporated using a pressure of $1.0 \times 10^{-6}$ mbar on top of the spiro-OMeTAD film using a shadow mask. The overlap between the ITO and Au electrodes determines the active area of the devices, which was 0.16 $cm^2$. Devices were measured with a shadow mask of 0.09 $cm^2$ to better define the active area. Blade coating was performed using a blade-coater Coatmaster 509 MC-I (from Erichsen Gmb, Germany), with the speed of 3 m/min. After the blade coating the spiro-OMeTAD layer was dried at room temperature to allow solvent evaporation. Thicknesses of the HTM were measured by wiping a small portion of the layer and by measuring the step edge with a Bruker profilometer.

**Device Characterization.** The *J*−*V* measurements were carried out in an $N_2$ environment under the simulated air mass (AM) 1.5G sunlight condition, using a tungsten−halogen lamp (~100 mW $cm^{-2}$) and a Keithley 2400 source meter. Devices were measured in both forward and reverse directions with a scan rate of 300 mV/s and then were tracked at the maximum power point (MPPT) for >120 s in order to get the stabilized efficiency values. The current density in the devices was checked with the help of EQE measurements. Typical *JV* curves of the devices, corresponding EQE measurement, and integrated current density of one typical device are shown in Figure S5. SEM images and EDX maps were acquired with a Jeol JSM-6010LA IntouchScope microscope.

## ASSOCIATED CONTENT

### Supporting Information

The Supporting Information is available free of charge on the ACS Publications website at DOI: 10.1021/acsaem.8b01122.

PV characteristics ($V_{oc}$, $J_{sc}$, FF, and PCE) of devices with various spin speeds and various annealing temperatures of spiro-OMeTAD and manufactured by blade coating. SEM analysis of spiro-OMeTAD layer, and typical *JV* curves and corresponding EQE measurements with integrated $J_{sc}$ (PDF)

## AUTHOR INFORMATION


### Corresponding Author

*E-mail: yulia.galagan@tno.nl.

### ORCID

Francesco Di Giacomo: 0000-0002-2489-5385

Yulia Galagan: 0000-0002-3637-5459


### Notes

The authors declare no competing financial interest.

## ACKNOWLEDGMENTS

This work has been supported by Solliance, a partnership of R&D organizations from The Netherlands, Belgium, and Germany working in thin film photovoltaic solar energy. This work is part of the research programme CLEARPV, Grant M-



DOI: 10.1021/acsaem.8b01122
ACS Appl. Energy Mater. 2018, 1, 6056−6063

ERA.NET 2017 CW with Project No. 732.017.105, which is (partly) financed by The Netherlands Organisation for Scientific Research (NWO).

## REFERENCES

(1) Kaushika, N. D.; Mishra, A.; Rai, A. K. Introduction to Solar Photovoltaic Power. *Solar Photovoltaics: Technology, System Design, Reliability and Viability*; Springer: Cham, Switzerland, 2018; pp 1−14, DOI: 10.1007/978-3-319-72404-1_1.

(2) Ma, X.; Yu, X.; Fan, R.; Yang, D. Formation of pnp bipolar structure by thermal donors in nitrogen-containing p-type Czochralski silicon wafers. *Appl. Phys. Lett.* **2002**, *81*, 496−498.

(3) Correa-Baena, J.-P.; Saliba, M.; Buonassisi, T.; Grätzel, M.; Abate, A.; Tress, W.; Hagfeldt, A. Promises and challenges of perovskite solar cells. *Science* **2017**, *358*, 739−744.

(4) Chen, Q.; De Marco, N.; Yang, Y.; Song, T.-B.; Chen, C.-C.; Zhao, H.; Hong, Z.; Zhou, H.; Yang, Y. Under the spotlight: The organic−inorganic hybrid halide perovskite for optoelectronic applications. *Nano Today* **2015**, *10*, 355−396.

(5) Im, J.-H.; Lee, C.-R.; Lee, J.-W.; Park, S.-W.; Park, N.-G. 6.5% efficient perovskite quantum-dot-sensitized solar cell. *Nanoscale* **2011**, *3*, 4088−4093.

(6) National Research Energy Laboratory (NREL). *Best Research−Cell Efficiencies*, https://www.nrel.gov/pv/assets/images/efficiency-chart.png, 2018.

(7) Razza, S.; Castro-Hermosa, S.; Di Carlo, A.; Brown, T. M. Research Update: Large-area deposition, coating, printing, and processing techniques for the upscaling of perovskite solar cell technology. *APL Mater.* **2016**, *4*, 091508.

(8) Song, Z.; McElvany, C. L.; Phillips, A. B.; Celik, I.; Krantz, P. W.; Watthage, S. C.; Liyanage, G. K.; Apul, D.; Heben, M. J. A technoeconomic analysis of perovskite solar module manufacturing with low-cost materials and techniques. *Energy Environ. Sci.* **2017**, *10*, 1297−1305.

(9) Priyadarshi, A.; Haur, L. J.; Murray, P.; Fu, D.; Kulkarni, S.; Xing, G.; Sum, T. C.; Mathews, N.; Mhaisalkar, S. G. A large area (70 cm2) monolithic perovskite solar module with a high efficiency and stability. *Energy Environ. Sci.* **2016**, *9*, 3687−3692.

(10) Di Giacomo, F.; Shanmugam, S.; Fledderus, H.; Bruijnaers, B. J.; Verhees, W. J. H.; Dorenkamper, M. S.; Veenstra, S. C.; Qiu, W.; Gehlhaar, R.; Merckx, T.; Aernouts, T.; Andriessen, R.; Galagan, Y. Up-scalable sheet-to-sheet production of high efficiency perovskite module and solar cells on 6-in. substrate using slot die coating. *Sol. Energy Mater. Sol. Cells* **2018**, *181*, 53−59.

(11) Galagan, Y.; Coenen, E. W. C.; Verhees, W. J. H.; Andriessen, R. Towards the scaling up of perovskite solar cells and modules. *J. Mater. Chem. A* **2016**, *4*, 5700−5705.

(12) Noel, N. K.; Habisreutinger, S. N.; Wenger, B.; Klug, M. T.; Horantner, M. T.; Johnston, M. B.; Nicholas, R. J.; Moore, D. T.; Snaith, H. A Low Viscosity, Low Boiling Point, Clean Solvent System for the Rapid Crystallisation of Highly Specular Perovskite Films. *Energy Environ. Sci.* **2017**, *10*, 145−152.

(13) Gardner, K. L.; Tait, J. G.; Merckx, T.; Qiu, W.; Paetzold, U. W.; Kootstra, L.; Jaysankar, M.; Gehlhaar, R.; Cheyns, D.; Heremans, P.; Poortmans, J. Nonhazardous Solvent Systems for Processing Perovskite Photovoltaics. *Adv. Energy Mater.* **2016**, *6*, 1600386.

(14) Wang, J.; Di Giacomo, F.; Brüls, J.; Gorter, H.; Katsouras, I.; Groen, P.; Janssen, R. A. J.; Andriessen, R.; Galagan, Y. Highly Efficient Perovskite Solar Cells Using Non-Toxic Industry Compatible Solvent System. *Solar RRL* **2017**, *1*, 1700091.

(15) Khenkin, M. V.; K. M., A.; Visoly-Fisher, I.; Kolusheva, S.; Galagan, Y.; Di Giacomo, F.; Vukovic, O.; Patil, B. R.; Sherafatipour, G.; Turkovic, V.; Rubahn, H.-G.; Madsen, M.; Mazanik, A. V.; Katz, E. A. Dynamics of Photoinduced Degradation of Perovskite Photovoltaics: From Reversible to Irreversible Processes. *ACS Appl. Energy Mater.* **2018**, *1*, 799−806.

(16) Bu, T.; Wu, L.; Liu, X.; Yang, X.; Zhou, P.; Yu, X.; Qin, T.; Shi, J.; Wang, S.; Li, S.; Ku, Z.; Peng, Y.; Huang, F. Z.; Meng, Q.; Cheng, Y.-B.; Zhong, J. Synergic Interface Optimization with Green Solvent Engineering in Mixed Perovskite Solar Cells. *Adv. Energy Mater.* **2017**, *7*, 1700576.

(17) Yavari, M.; Mazloum-Ardakani, M.; Gholipour, S.; Tavakoli, M. M.; Turren-Cruz, S.-H.; Taghavinia, N.; Gratzel, M.; Hagfeldt, A.; Saliba, M. Greener, Nonhalogenated Solvent Systems for Highly Efficient Perovskite Solar Cells. *Adv. Energy Mater.* **2018**, *8*, 1800177.

(18) Hansen, C. M. *Hansen Solubility Parameters: A User's Handbook*, 2nd ed.; Taylor & Frances: London, 2007.

(19) Wang, S.; Sina, M.; Parikh, P.; Uekert, T.; Shahbazian, B.; Devaraj, A.; Meng, Y. S. Role of 4-tert-Butylpyridine as a Hole Transport Layer Morphological Controller in Perovskite Solar Cells. *Nano Lett.* **2016**, *16*, 5594−5600.

(20) Occupational Safety and Health Administration, United States Department of Labor. https://www.osha.gov/, 2018.

(21) Grancini, G.; Roldán-Carmona, C.; Zimmermann, I.; Mosconi, E.; Lee, X.; Martineau, D.; Narbey, S.; Oswald, F.; De Angelis, F.; Graetzel, M.; Nazeeruddin, M. K. One-Year stable perovskite solar cells by 2D/3D interface engineering. *Nat. Commun.* **2017**, *8*, 15684.

(22) Shen, Q.; Ogomi, Y.; Chang, J.; Tsukamoto, S.; Kukihara, K.; Oshima, T.; Osada, N.; Yoshino, K.; Katayama, K.; Toyoda, T.; Hayase, S. Charge transfer and recombination at the metal oxide/CH3NH3PbClI2/spiro-OMeTAD interfaces: uncovering the detailed mechanism behind high efficiency solar cells. *Phys. Chem. Chem. Phys.* **2014**, *16*, 19984−19992.

(23) Jena, A. K.; Chen, H.-W.; Kogo, A.; Sanehira, Y.; Ikegami, M.; Miyasaka, T. The Interface between FTO and the TiO2 Compact Layer Can Be One of the Origins to Hysteresis in Planar Heterojunction Perovskite Solar Cells. *ACS Appl. Mater. Interfaces* **2015**, *7*, 9817−9823.

(24) Yang, D.; Zhou, X.; Yang, R.; Yang, Z.; Yu, W.; Wang, X.; Li, C.; Liu, S.; Chang, R. P. H. Surface optimization to eliminate hysteresis for record efficiency planar perovskite solar cells. *Energy Environ. Sci.* **2016**, *9*, 3071−3078.

(25) Zhou, H.; Chen, Q.; Li, G.; Luo, S.; Song, T.-b.; Duan, H.-S.; Hong, Z.; You, J.; Liu, Y.; Yang, Y. Interface engineering of highly efficient perovskite solar cells. *Science* **2014**, *345*, 542−546.

(26) Jena, A. K.; Numata, Y.; Ikegami, M.; Miyasaka, T. Role of spiro-OMeTAD in performance deterioration of perovskite solar cells at high temperature and reuse of the perovskite films to avoid Pb-waste. *J. Mater. Chem. A* **2018**, *6*, 2219−2230.

(27) Jena, A. K.; Ikegami, M.; Miyasaka, T. Severe Morphological Deformation of Spiro-OMeTAD in (CH3NH3)PbI3 Solar Cells at High Temperature. *ACS Energy Lett.* **2017**, *2*, 1760−1761.

(28) Saliba, M.; Matsui, T.; Seo, J.-Y.; Domanski, K.; Correa-Baena, J.-P.; Nazeeruddin, M. K.; Zakeeruddin, S. M.; Tress, W.; Abate, A.; Hagfeldt, A.; Gratzel, M. Cesium-containing triple cation perovskite solar cells: improved stability, reproducibility and high efficiency. *Energy Environ. Sci.* **2016**, *9*, 1989−1997.



DOI: 10.1021/acsaem.8b01122
*ACS Appl. Energy Mater.* 2018, 1, 6056−6063